Desalination and Water Treatment
www.deswater.com

doi: 10.5004/dwt.2023.29802

304 (2023) 112–128
August

Prediction of climate change on surface water using NARX neural network model: a case study on Ghezel Ozan River, Northwest, Iran

Sadegh Mohammadi[a], Soodeh Karimi[b], Ali Akbar Mohammadi[c], Soheila Moghanlo[a], Mehrdad Alavinejad[d], Hossein Najafi Saleh[e], Hamed Mohammadi[a,*], Mehdi Nezam Hashemi[f], Ozgur Kisi[g,h]

[a]*Department of Environmental Health Engineering, School of Public Health, Zanjan University of Medical Sciences, Zanjan, Iran, emails: ham19@zums.ac.ir (H. Mohammadi), sadeghmohamadiii61@gmail.com (S. Mohammadi), moghanlosoheila14@gmail.com (S. Moghanlo)*
[b]*Department of Environmental Health Engineering, School of Public Health, Shahid Beheshti University of Medical Sciences, Tehran, Iran, email: soodehkarimii66@gmail.com (S. Karimi)*
[c]*Department of Environmental Health Engineering, Neyshabur University of Medical Sciences, Neyshabur, Iran, email: Mohammadi.eng73@gmail.com (A.A. Mohammadi)*
[d]*Academic Center for Education, Culture and Research of Zanjan, Zanjan, Iran, email: mehrdad.alavinejad@gmail.com (M. Alavinejad)*
[e]*Department of Environmental Health Engineering, Khalkhal University of Medical Sciences, Khalkhal, Iran, email: najafi.saleh@gmail.com (H.N. Saleh)*
[f]*Department of Health, Safety and Environment Islamic Azad University Meybod Branch Meybod, Iran, email: mehdinezamhashemi@yahoo.com (M.N. Haeshmi)*
[g]*Department of Civil Engineering, Technical University of Lübeck, 23562 Lübeck, Germany, email: ozgur.kisi@th-luebeck.de (O. Kisi)*
[h]*Department of Civil Engineering, Ilia State University, 0162 Tbilisi, Georgia, email: ozgur.kisi@iliauni.edu.ge (O. Kisi)*

Received 25 March 2023; Accepted 16 July 2023

ABSTRACT

The quantity and quality of surface waters are affected by climate change. Therefore, the study of the impact of climate change on surface water is very important. In the first part of the study, the output of the HadGM2-ES model was used to generate a future climatic pattern under two Representative Concentration Pathway (RCP) scenarios: RCP2.6 and RCP8.5. The atmospheric circulation data from the model were utilized for this purpose. In the second part of the study, the climate model Long Ashton Research Station Weather Generator (LARS-WG) was employed to downscale climate data, including precipitation flow, temperatures, total solids (TS), and electrical conductivity (EC) parameters of the Ghezel Ozan River until 2050. In the final section, we evaluated the NARX neural network model for simulating the quality and quantity parameters. The results proved that the LARS-WG software has an extraordinary ability to downscale and generate synthetic series of climatic variables. According to the emission scenarios RCP2.6 and RCP8.5, an increasing trend in minimum and maximum temperature was predicted over the future time period. The highest temperature was obtained under the worst situation of RCP8.5. Additionally, the results showed that the highest decrease in precipitation is estimated as 15.38% in mid-winter and 18.68% in early spring during the future period. With the decrease in precipitation, the river flow is projected to decrease by 42.59% in late winter and 76.32% in early spring compared to the observation period. As a result of decreased precipitation and discharge, the EC parameter is expected to increase by 52.06% in late winter and 81.27% in early spring compared to the base period. Overall, our findings indicate that these parameters are strongly influenced by climate change, posing a risk of water shortage and drought to the ecosystem of many aquatic organism's dependent on this river.

Keywords: Climate change; Simulation; NARX Tarom; Ghezel Ozan River

* Corresponding author.

1. Introduction

Today, due to increased population and subsequent surges in water demand, the effects of climate change require more precise integrated management than ever to meet water consumption in various fields such as agriculture, sanitation, and industry [1,2]. Climate change is a critical factor known to impact the environment significantly. The primary effects of climate change on water quality and quantity are attributed to variations in air temperature and precipitation patterns. Changes in the timing, amount, and location of rainfall pose threats to ecosystems and wildlife species [3]. Furthermore, the projected increase in greenhouse gases and the resulting intensification of changes in climatic parameters can have numerous negative effects on various systems, including water resources, the environment, industry, health, agriculture, and all systems that interact with the climate system [4]. With climate change, the hydrological regime of rivers and streams may indicate an increased risk of floods [5]. The impact of climate change on surface water, particularly rivers, tends to decrease the quality of drinking water, leading to increased health risks, especially during extreme weather events [6]. Examining trends in hydrological time series can be effective in interpreting the relationship between processes and environmental changes in the study areas. Changes in temperature in rivers and lakes can influence the water quality of these resources [7,8]. Given the significance of the impact of global warming and climate change on river water resources, it is both useful and necessary to investigate the behavior of rivers, particularly water levels, in the future periods under the influence of these phenomena. This will aid in water resource management and provide solutions to mitigate the deteriorating effects of climate change [9,10]. The 4th Assessment Report of the Intergovernmental Panel on Climate Change (IPCC) indicated that air temperature has increased by an average of 0.74°C over the past 100 y (1906–2007) compared to the average of the previous 30 y (1982). According to the 5th report, the temperature increase reached 0.85°C [11,12]. Global warming and climate change are highly associated with human activities. These issues are major environmental problems that have attracted the attention of many scientists and policymakers around the world in recent years [13,14]. The main impacts of climate change related to water quality parameters include the alteration of surface water levels in rivers and lakes, as well as the values of quality parameters (pathogenic microorganisms, physicochemical, and biological indicators), leading to an increased risk situation in terms of potential health impacts [15,16]. Therefore, predicting the qualitative and quantitative parameters of water along the river for the purpose of management decisions is considered one of the goals of water resource managers and planners [17]. In this context, models based on differential equations have provided accurate predictions by using a data-driven approach to identify the optimal input and output mapping [18]. Hydrological modeling to simulate the quality of water resources in the present and future requires an understanding of global climate models (GCM), emission scenarios, and downscaling GCM output reduction. GCMs produce results at a relatively coarse temporal resolution, in many cases too coarse to capture water quality dynamics. Therefore, resampling of the data is required to generate data at sub-daily temporal resolution [19,20]. Recent research has shown that data-driven models provide accurate predictions [19]. However, most of these models cannot investigate the nonlinear dynamics inherent in meteorological phenomena, so they may not always perform well and provide the intended acceptable forecast [21]. To achieve these goals, it is inevitable to use Artificial Intelligence (AI) and Machine Learning (ML). ML methods have been proposed as an alternative for modeling nonlinear and dynamic systems. ML methods have been applied in various research fields, such as finance, agriculture, and weather prediction, with acceptable accuracy. They can automatically extract image features of extreme weather phenomena and predict the possibility of extreme weather events using a deep learning framework [21]. Weather generators have become highly useful tools for capturing variability and uncertainty associated with climate change, particularly in the context of water quality [22,23]. Statistical downscaling methods (SDSMs) and regional climate models (RCMs) have been applied for climate change prediction [22]. The Long Ashton Research Station Weather Generator (LARS-WG) falls under the category of SDSM. Researchers have examined LARS-WG for downscaling climate data, including rainfall, solar radiation, minimum stream flow, crop and sediment yields, and maximum temperature [24–27]. In recent decades, the use of artificial neural networks (ANNs) has become common in many engineering sciences for simulating and predicting various phenomena [28–30]. ANNs have also been successfully applied in both short-term and long-term predictions [31]. ANNs are techniques with flexible mathematical structures that can identify complex nonlinear relationships between input and output data [32]. Emamgholizadeh et al. [33] utilized ANNs to predict water quality in the Karoon River. Gazzaz et al. [34,35] conducted a study in Malaysia using water quality predictors and ANNs to model the water quality index of the Quinta River. Sulaiman et al. [36] performed a study focused on the classification of water quality characteristics. In order to estimate TDS and EC in Abu-Ziriq marsh south of Iraq, Al-Mukhtar et al. [37] used the adaptive neural fuzzy inference system (ANFIS), ANN, and multiple regression (MLR) models. Furthermore, Kadam et al. [38] examined the application of ANN and MLR techniques for predicting drinking groundwater in the Western Ghat region of India. Based on numerous previous studies, the neural network model proves to be a valid and accurate method for simulating water quality. Fundamentally, one of the most important steps in implementing and meeting the needs of integrated water resource management in large watersheds is the optimal sharing of surface water [39].

Due to factors such as population growth, industrial expansion, climate change, and decreasing precipitation in various regions, there has been a decline in the flow of river water. Consequently, predicting the impact of climate change on surface water is crucial for effective water resource management in the future. While existing research demonstrates the significant influence of climate change on the quality and quantity of surface water resources, no studies have specifically focused on predicting the effects of climate change on the Ghezel Ozan River. The Ghezel Ozan-Safid River watershed, covering an area of 5,900 km^2, is one of the most important aquatic ecosystems in northwest Iran.

It profoundly affects the residents of Zanjan, Gilan, Qazvin, Kurdistan, East Azerbaijan, Ardabil, Hamedan, and Tehran provinces in terms of economy, society, and agriculture. The river has experienced severe water resource crises, including floods and droughts, in recent years. Hence, projecting the changes in surface water resources under future climate scenarios plays a crucial role in shaping water resource management strategies for this region. The main objectives of this study are as follows: (1) To generate future climatic patterns under two scenarios, namely RCP2.6 and RCP8.5. Meteorological data, including precipitation, minimum and maximum temperatures, were measured and recorded at the Tarom Synoptic Station over the past 20 y. (2) To employ the LARS-WG model for downscaling and validating the data. Future meteorological data spanning from 2021 to 2050 were extracted from the IPCC and DDC for a 30-y period. (3) To utilize the NARX neural network model for predicting stream flow, precipitations, EC (electrical conductivity), and TS (total solids) of the Ghezel Ozan River by 2050. These parameters are vital for assessing water quality in terms of drinking and agricultural sectors, respectively, under climate change conditions. The findings of this research will play a significant role in the management and control of surface water resources in the region.

2. Material and methods

2.1. Study of area

Tarom city is situated in the northern part of Zanjan province and is one of its eight cities. The city spans an area of over 2235 km^2, located between 48°30′ and 49°14′ longitude and 36°38′ and 37°13′ north latitude. Within the city, there are 22 rivers originating from the surrounding mountains that eventually join the Ghazal Ozen River. The catchment area of this river measures 49,500 km^2. The average annual rainfall in Tarom city is 200 mm, with the majority of precipitation occurring during the winter season. The Abhar meteorological observatory station, located in Tarom city, records an average minimum temperature of 11.6°C and an average maximum temperature of 32.2°C. Furthermore, the annual average temperature in the city is 17.5°C, with the absolute maximum and minimum temperatures recorded at 48°C and –9.5°C, respectively (Fig. 1) [40].

2.2. Data collection

Meteorological data, including daily minimum temperature (T_{min}), daily maximum temperature (T_{max}), and daily precipitation (P), were obtained from the documents provided by Tarom Meteorological Organization over a period of 20 y. These data were extracted on a daily basis from the Tarom Synoptic Station (Table 1). Additionally, EC, TS, and discharge data recorded by the Gilvan Hydroclimate Station were acquired from the Gilan Regional Water Company for the period from 1990 to 2020. The collected data were subsequently normalized and verified using MATLAB software.

2.3. Micro scaling and simulation of observed data

The prediction of future climate variables using global climate models (GCM) under different emission scenarios is valuable for understanding the current situation and developing strategies to adapt to climate change. Weather generators have emerged as powerful tools for capturing the variability and uncertainty associated with climate change. Among these tools, AOGCM numerical models are considered the best method for evaluating the impacts of climate change [41]. These models simulate physical processes in the atmosphere, ocean, cryosphere, and Earth's surface, enabling

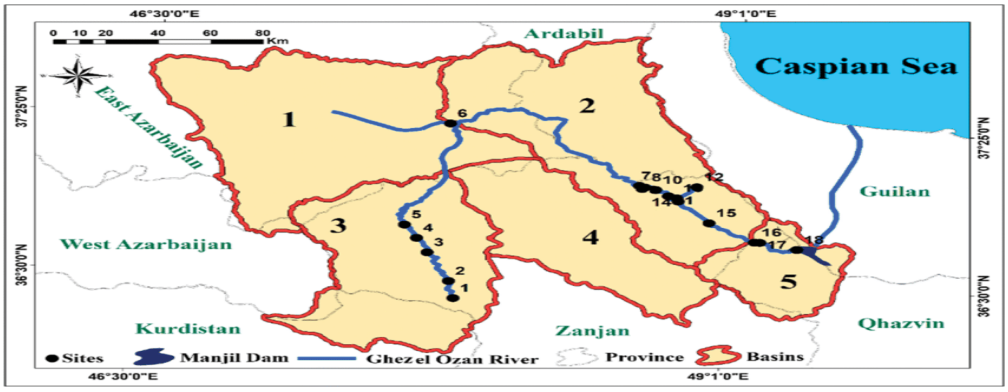

Fig. 1. The Ghezel Ozan River in relation to the provinces and the catchment area [40].

Table 1
Details of stations used in this study

Stations	Sampling sites	Longitude	Latitude	Elevations (m above sea level)	*Riverbed conditions*
1	Darram	48° 44′ E	37° 01′ N	397	Non-coarse rubble, sand, silt and clay
2	Kuh Kan-e Sofla	48° 55′ E	36° 53′ N	376	
3	Gilvan	49° 08′ E	36° 47′ N	337	

an understanding of how the world's climate changes due to increasing greenhouse gas concentrations. However, AOGCM models provide global climate projections and are unable to depict regional-scale climate changes. Therefore, downscaling techniques are necessary to predict climate changes on regional and local scales. One such downscaling method is the Long Ashton Research Station Weather Generator (LARS-WG), which is a statistical model [42]. In this study, microscaling techniques were employed to transfer climate information from large-scale climate models to microscale climate models [43]. Microscale methods like LARS-WG are crucial for improving the accuracy of outputs derived from GCM models [44]. For our analysis, we utilized the latest version of LARS-WG, namely LARS-WG 6.0. This software was used to perform exponential microscaling of water quality variables, including temperature and precipitation changes, under various scenarios for the period between 2021–2050. To generate these predictions, we utilized the output of the HadGM2-ES model from the CMIP5 model series, provided by the MOHC Research Institute. The two scenarios considered were RPC2.6 (optimistic) and RPC8.5 (pessimistic), as outlined in the 5th Report (AR5) of the IPCC [27].

2.4. Validation of data generated in LARS-WG

2.4.1. Data preparation and sorting

In this step, the data obtained from the Meteorological Organization was sorted using MATLAB software based on the input requirements of the LARS-WG software.

2.4.2. Basic data analysis

In this step, the statistical characteristics of the received data (observations) were defined and analyzed.

2.4.3. Primary data generation

In this step, artificial data generation was performed by the model for the base period, and the statistical characteristics of the generated artificial data were determined.

2.4.4. Statistical comparison

The observed and reproduced data were subjected to statistical analysis. *T*-tests, *F*-tests, and KS (Kolmogorov-Smirnov) statistical tests were utilized to assess the model's performance during the calibration period. The corresponding *p*-values for each month are also provided, allowing us to infer that there is a significant difference between the observed and simulated data based on these results.

2.4.5. Production of daily data in the future

To simulate the future climate conditions of the desired location, the model incorporated the RCP2.6 and RCP8.5 greenhouse gas emission scenarios, along with the output from climate models for the base period. Subsequently, reproduction and climate change were simulated using the LARS-WG software. The LARS-WG software generated projections for minimum and maximum temperatures, as well as precipitation in the study area until 2050. Following this, the impact of climate change on both the quality and quantity of water in the Qezal-Ozen River was examined. ANN techniques were employed to simulate and assess the effects of climate change on water quality and quantity [45].

2.5. Simulation of desired quantitative and qualitative parameters by artificial neural network

In general, the development stages of ANN models can be divided into eight stages [12,46]. These steps are:

(1) Data collection: The data for this study was collected from the Tarom Meteorological Department and Gilan District Water Department. This dataset encompasses 20 y of maximum and minimum temperatures, precipitation, TS, EC, and runoff data, spanning from 1990 to 2020.
(2) Data pre-processing: In the present study, the input data was normalized within a range between zero and one. Additionally, the linear interpolation method was employed using the nearest neighbors to fill in any missing data.

In order to ensure homogeneity, several steps were taken to address outlier values in the input data used for training and testing the NARX model. Firstly, a thorough examination of the input data was conducted to identify any potential outliers. Subsequently, appropriate methods were employed to handle these outliers, such as removing them or replacing them with more suitable values. One approach utilized involved replacing outlier values with the mean of neighboring values, considering the distribution of the data. Furthermore, the robustness of the NARX model was relied upon to handle small to moderate levels of outliers in the input data. This is attributed to the model's capability to capture non-linear relationships between variables and its inherent mechanism for noise reduction.

(3) Selection of input variables: A model-based procedure was employed in this study, where inputs were selected on a case-by-case basis. The selection process was guided by prior knowledge of the impacts of temperature, precipitation, and day of the year on watershed quantity and quality.
(4) Data classification: One of the data classification methods commonly employed in previous studies is the ad hoc method. An example of this method involves allocating 70% of the data for training, 15% for validation, and 15% for testing. In this particular study, the ad hoc method was utilized to categorize the data.
(5) Model architecture selection: A nonlinear autoregressive network model with extrinsic inputs (NARX) was employed to determine the model architecture. The NARX model is extensively utilized in air pollution prediction applications and is capable of capturing various nonlinear behaviors [47]. The formula for the NARX model can be expressed as a discrete-time recursive input-output equation as follows:

$$y(t) = f\left(y(t-1),\ldots,y\left(t-n_y\right),u(t-1),\ldots,y\left(t-n_y\right)\right)+\zeta(t)$$

where u is the input, y is the output, and ξ is the noise factor. NARX networks offer several advantages over linear models for time series prediction. One key advantage is their ability to capture complex nonlinear relationships between input and output data, which often leads to more accurate predictions. Additionally, NARX networks are known for their good generalization to new data points, making them useful for predicting future time steps. They are also easy to implement using neural network toolboxes like the one in MATLAB, and can be designed with flexible architectures to suit different types of time series prediction problems.

Given the high efficiency of the NARX architecture in predicting time series data, especially in cases involving air pollution and nonlinear input-output relationships, we implemented the NARX architecture using the neural network toolbox in MATLAB R2019b.

(6) Determining the structure of the model: In this study, the selection of the number of layers is based on the architecture of the NARX neural network toolbox in MATLAB software. In our model structure, there are three layers for inputs, outputs, and hidden nodes. The neurons in the input and output layers were automatically determined using MATLAB software, considering the number of inputs and outputs. However, the number of neurons in the middle layer was selected through a trial and error method in this study. By adjusting the weights and biases, the neural network can establish an accurate mapping between the input neurons and the output. ANN training typically follows a supervised approach.
(7) Model training: Before applying ANN models for prediction, it is necessary to train or calibrate the models. During training, adjustments are made to the weights of each connection between the neurons in the network. Additionally, prior to training, the weights and biases of the network are typically initialized. The initial weight values are randomly selected from a uniform distribution [48]. In this study, we utilized the Bayesian method available in the MATLAB neural network toolbox to train the model.
(8) Validation of ANN neural network models: To quantify the performance of ANN models, it is necessary to consider various statistical performance indicators. Typically, the performance of an ANN model is assessed using a quantitative error measure that encompasses three significant aspects of validity: repeatable validity, predictive validity, and structural validity.

2.6. Artificial neural network implementation

The objective of implementing the neural network in this study was to predict the TS, EC, and discharge of the Ghazal Ozen River from 2021 to 2050. This prediction was based on the available data concerning temperature and precipitation, which were generated by the LARS software during the specified period. As discussed earlier, the NARX architecture provided by the MATLAB Neural Networks Toolbox was employed for this investigation (Fig. 2).

Out of the entire dataset, 70% was allocated for training, while 15% each was assigned for validation and testing purposes. The performance of the network was evaluated using metrics such as mean squared error and the mean of observed and generated regressions. Subsequently, the relationships between the main variables obtained from the models were examined. The models were developed through training artificial neural networks (ANNs). Additionally, the impact of the inputs on the outputs was assessed, and the model was selected based on evaluation criteria.

3. Results

3.1. Microscale climate change

The findings of the microscale climate change analysis indicate a close agreement between the average observed and produced precipitation data by LARS software. The mean standard deviation of precipitation, calculated over several years, aligns in late spring, summer, and late winter (Fig. 3a and b). Additionally, the average minimum and maximum temperature data obtained from observations and generated by LARS exhibit a high level of consistency and similarity. However, the mean standard deviation of simulated temperature data, calculated over multiple years, is lower than the observed mean standard deviation for all months (Fig. 4a and d). Overall, the LARS software demonstrates moderate performance for temperature simulations and good performance for precipitation simulations. The statistical model employed by LARS effectively examines the disparities between observed and generated data. The

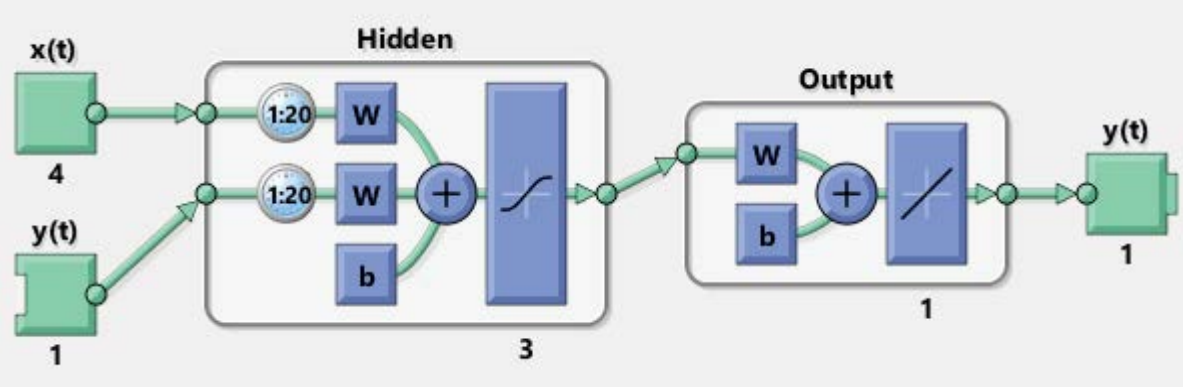

Fig. 2. Schematic of NARX neural network for predicting TS, EC and Q.

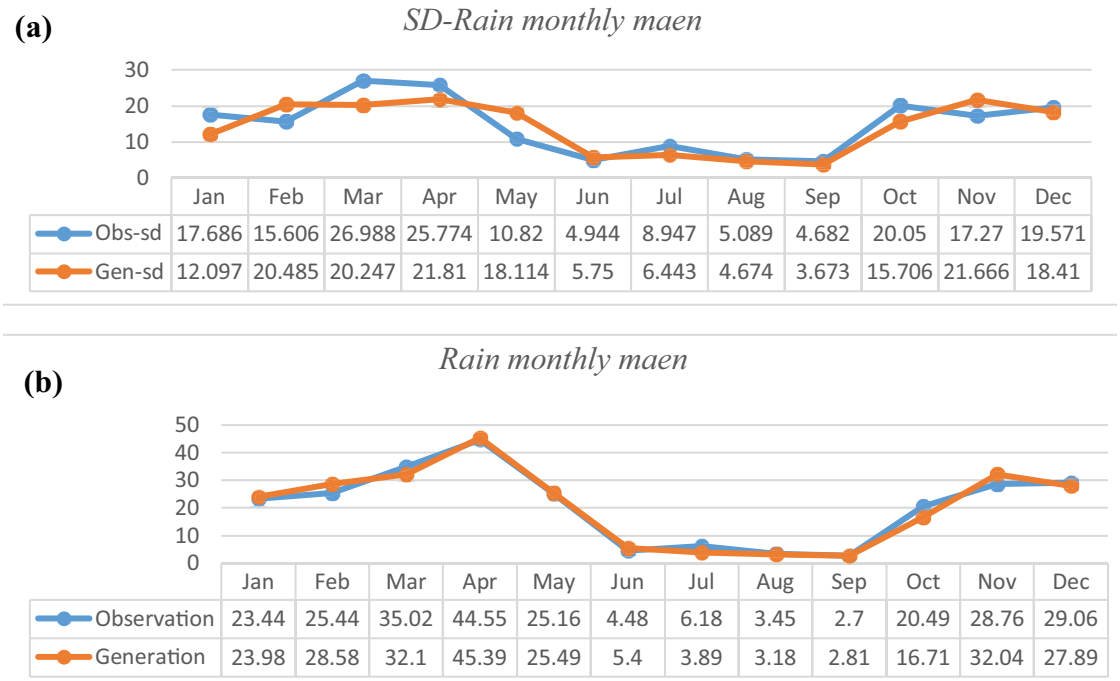

Fig. 3. Evaluation of (a) mean standard deviation (b) and observed simulated monthly precipitation in LARS-WG.

results of the investigations highlight the exceptional ability of the LARS software to generate synthetic series of climatic variables.

3.2. Findings of climate change simulation

Microscaling and data validation related to climate change were conducted using the LARS-WG software. The output data from the site analysis submenu, as well as the outputs of the HadGM2-ES model under the RCP2.6 and RCP8.5 scenarios, were utilized in the Generator menu to estimate the changes in minimum and maximum temperature and precipitation for the period from 2021 to 2050. Figs. 5 and 6 present the estimated atmospheric values (minimum and maximum temperature and precipitation) for the study area based on the RCP2.6 and RCP8.5 scenarios in the LARS software. The results demonstrate an increase in both the minimum and maximum temperatures for both scenarios by 2050. In Fig. 5a and b, the highest temperature increases are associated with the RCP8.5 scenario, with average temperature rises of at least 4.8°C. The most significant temperature increases occur in December (late autumn) and January, February, and March (winter) compared to the given period. Additionally, the average maximum temperature shows an increase of 1.28°C compared to the reference period (Fig. 5b). Regarding precipitation, the largest average increase is observed in all months for the RCP2.6 scenario. However, the maximum decreases in mean monthly precipitation under the RCP2.6 and RCP8.5 scenarios are noted in February (mid-winter) and April (early spring), with reductions of 15.38% and 18.68%, respectively. In contrast, the highest increases in average rainfall occur in December (late autumn) and January (early winter), with percentages of 29.87% and 29.87% in the RCP2.6 scenario, and 20.43% and 25.97% in the RCP8.5 scenario, respectively. Overall, mean precipitation increases for most months in both scenarios throughout the period, except for February and March (late winter) and April (early spring) (Fig. 6).

Figs. 7 and 8 present the regionally generated atmospheric values, including minimum and maximum temperatures and precipitation, based on the RCP2.6 and RCP8.5 scenarios over a 30-y period from 2021 to 2050. The results indicate that both the minimum and maximum temperatures increase by 2050 for both scenarios. In terms of the annual mean minimum and maximum temperatures, the RCP8.5 scenario exhibits the highest level of warming, with an annual mean minimum temperature of 4.6°C. In comparison, the RCP2.6 scenario shows a lower warming level with an annual mean minimum temperature of 4.9°C during the observation period (Fig. 7a). Additionally, Fig. 7b illustrates that the annual mean temperature rises by 0.99°C in the RCP2.6 scenario and by 1.38°C in the RCP8.5 scenario compared to the reference period. Annual precipitation displays variations throughout the year. The highest average annual rainfall is projected to occur in 2023, 2025, 2036, 2043, and 2045 (Fig. 8). Moreover, Fig. 8 indicates that the average annual precipitation increases by 2.7% in the RCP2.6 scenario and by 2.89% in the RCP8.5 scenario compared to the observation period.

3.3. Neural network findings

The NARX neural network was employed in this study. The main inputs of the network include minimum temperature, maximum temperature, precipitation, day of the year, and a discharge-related input. One of the significant advantages of NARX networks is their ability to consider the influence of previous inputs and outputs on the current

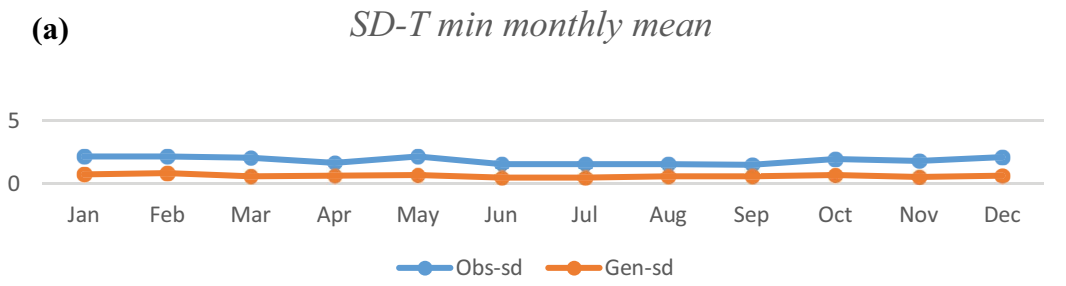

(b) *T min monthly mean*

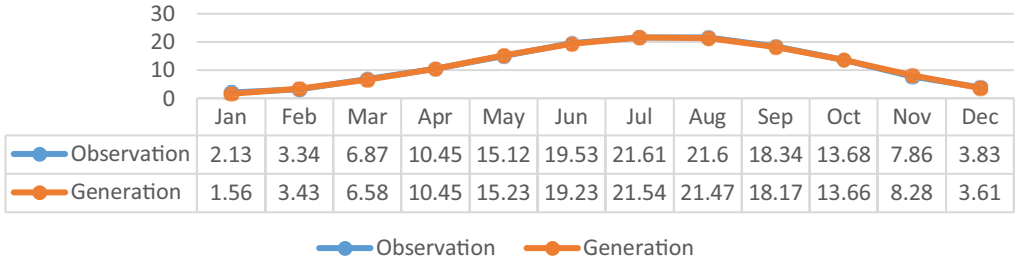

	Jan	Feb	Mar	Apr	May	Jun	Jul	Aug	Sep	Oct	Nov	Dec
Observation	2.13	3.34	6.87	10.45	15.12	19.53	21.61	21.6	18.34	13.68	7.86	3.83
Generation	1.56	3.43	6.58	10.45	15.23	19.23	21.54	21.47	18.17	13.66	8.28	3.61

(c) *SD-T max monthly mean*

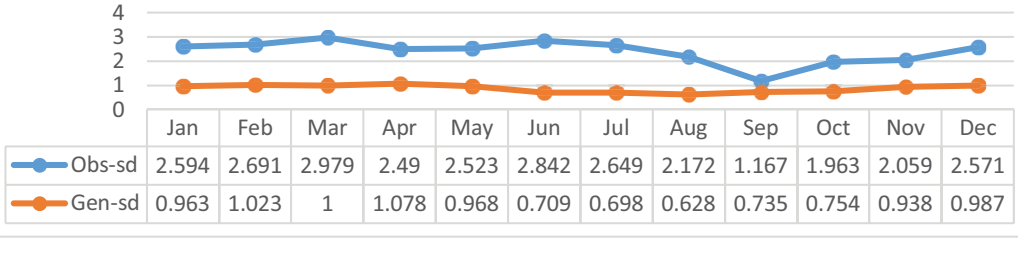

	Jan	Feb	Mar	Apr	May	Jun	Jul	Aug	Sep	Oct	Nov	Dec
Obs-sd	2.594	2.691	2.979	2.49	2.523	2.842	2.649	2.172	1.167	1.963	2.059	2.571
Gen-sd	0.963	1.023	1	1.078	0.968	0.709	0.698	0.628	0.735	0.754	0.938	0.987

(d) *T max monthly mean*

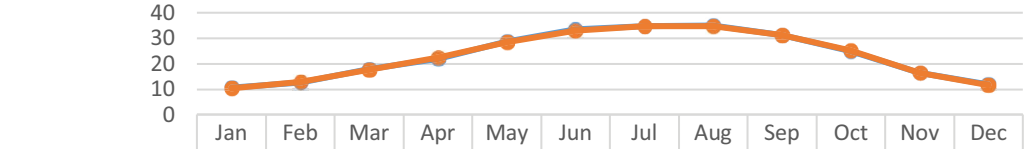

	Jan	Feb	Mar	Apr	May	Jun	Jul	Aug	Sep	Oct	Nov	Dec
Observation	10.64	12.55	18	21.94	28.73	33.47	34.87	34.93	31.24	24.85	16.5	11.81
Generation	10.3	12.96	17.75	22.48	28.41	33.01	34.75	34.64	31.11	25.3	16.44	11.55

Fig. 4. Evaluation of (a,c) mean standard deviation (b,d) and observed simulated monthly minimum and maximum temperature in LARS-WG.

output. To account for the daily effects of the previous day's discharge on the current discharge, 20 samples were selected. The mean squared error results generated by the network are presented in Fig. 9a, our findings indicate that the best validation result, with a value of 1.358×10^{-6}, was achieved during the fifty-fourth iteration of the network using MATLAB software. At this stage, the training error stood at 715.2×10^{-6}, the validation error at 1.358×10^{-6}, and the test error at 5.698×10^{-6}. Fig. 9b, illustrates the flowchart depicting the relationship between time and mean squared error. The accuracy of the network increases as the training production data aligns with the observation data. Therefore, the mean squared error of the output should approach zero. In our designed network, an acceptable value of 1.358×10^{-6} was attained, indicating a close match between the predicted data and the observed data. Additionally, Fig. 9c, presents a regression plot, demonstrating a correlation coefficient of 0.9999 during the training and testing phases.

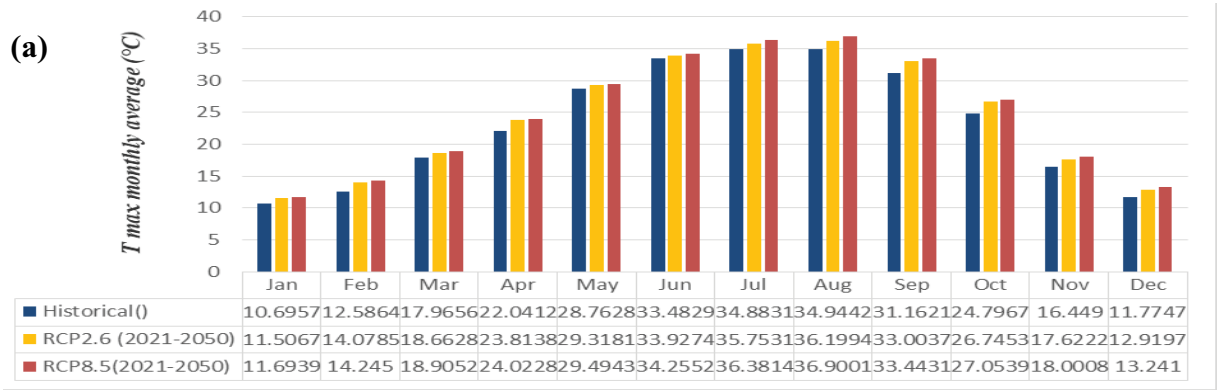

	Jan	Feb	Mar	Apr	May	Jun	Jul	Aug	Sep	Oct	Nov	Dec
Historical()	10.6957	12.586	17.965	22.041	28.762	33.482	34.883	34.944	31.162	24.7967	16.449	11.7747
RCP2.6 (2021-2050)	11.5067	14.078	18.662	23.813	29.318	33.927	35.753	36.199	33.003	26.745	17.622	12.9197
RCP8.5(2021-2050)	11.6939	14.245	18.905	24.022	29.494	34.255	36.381	36.900	33.443	27.053	18.0008	13.241

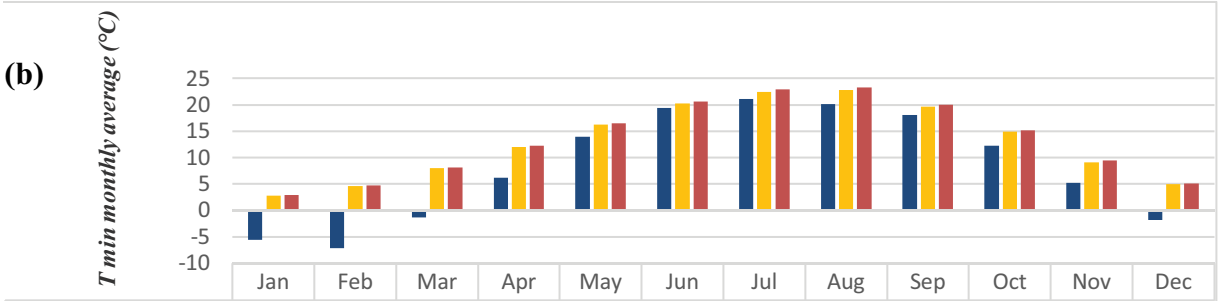

	Jan	Feb	Mar	Apr	May	Jun	Jul	Aug	Sep	Oct	Nov	Dec
Historical()	-5.532	-7.184	-1.282	6.1908	13.899	19.367	21.059	20.13	18.07	12.209	5.1542	-1.811
RCP2.6 (2021-2050)	2.7432	4.5728	7.9822	11.975	16.285	20.29	22.494	22.83	19.632	14.916	9.1183	4.9239
RCP8.5(2021-2050)	2.8763	4.7068	8.1644	12.212	16.553	20.631	22.985	23.328	19.998	15.206	9.4061	5.1354

Fig. 5. Monthly maximum (a) and minimum (b) temperature changes under two RCPs scenarios.

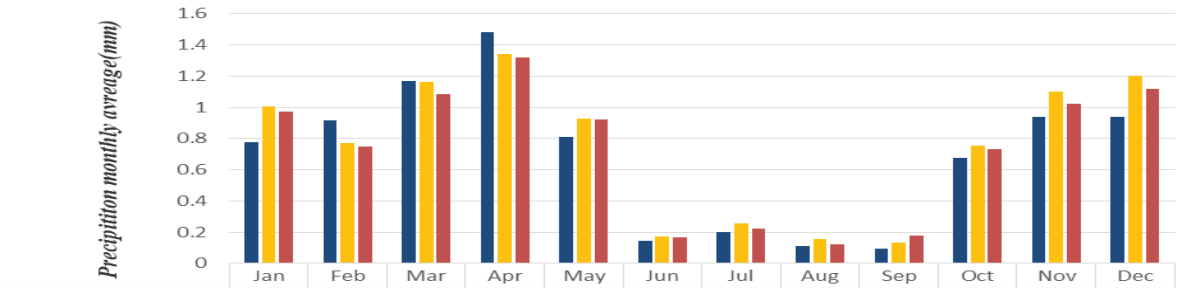

	Jan	Feb	Mar	Apr	May	Jun	Jul	Aug	Sep	Oct	Nov	Dec
Historical()	0.77644	0.91531	1.16602	1.48419	0.80947	0.14617	0.19932	0.11165	0.09627	0.67447	0.93905	0.93689
RCP2.6 (2021-2050)	1.00774	0.77191	1.16183	1.344	0.92989	0.17222	0.25538	0.15366	0.13644	0.75656	1.099	1.20269
RCP8.5(2021-2050)	0.97473	0.74845	1.08634	1.31822	0.92398	0.16744	0.22086	0.12312	0.17911	0.73495	1.02278	1.12118

Fig. 6. Monthly mean precipitation changes under two RCPs scenario.

This high correlation signifies a strong agreement between the data predicted by the network and the observed data.

After completing the training and testing phases and validating the accuracy of the designed neural network, the data was inputted into the neural network to predict the discharge for the 30-y period from 2021 to 2050. The annual and monthly average discharges were calculated for the RCP2.6 and RCP8.5 scenarios and are presented in Figs. 10 and 11. Fig. 8 displays the simulated discharge flow rate in the studied basin under the RCP2.6 and RCP8.5 scenarios from 2021 to 2050, allowing for comparison with observations. It was observed that runoff is projected to decrease by 2050 in both scenarios when compared to the observed data. The largest decreases in the average monthly discharge occurred in March (late winter), April, and May (early spring), with reductions of 42.59%, 76.32%, and 78.14%, respectively (Fig. 10). Additionally, in both scenarios, the overall amount of discharge displayed lower values compared to the observed data. The largest decrease in the average annual discharge was estimated to be 20 m^3/s in 2048 as an annual average. According to Fig. 11, the flow experienced a yearly reduction of 49.51% and 50.31% in the RCP2.6 and RCP8.5 scenarios, respectively, in comparison to the observation period. In general, the average monthly discharge values decreased during late spring, summer, and early autumn in the study basin, as shown in Fig. 12.

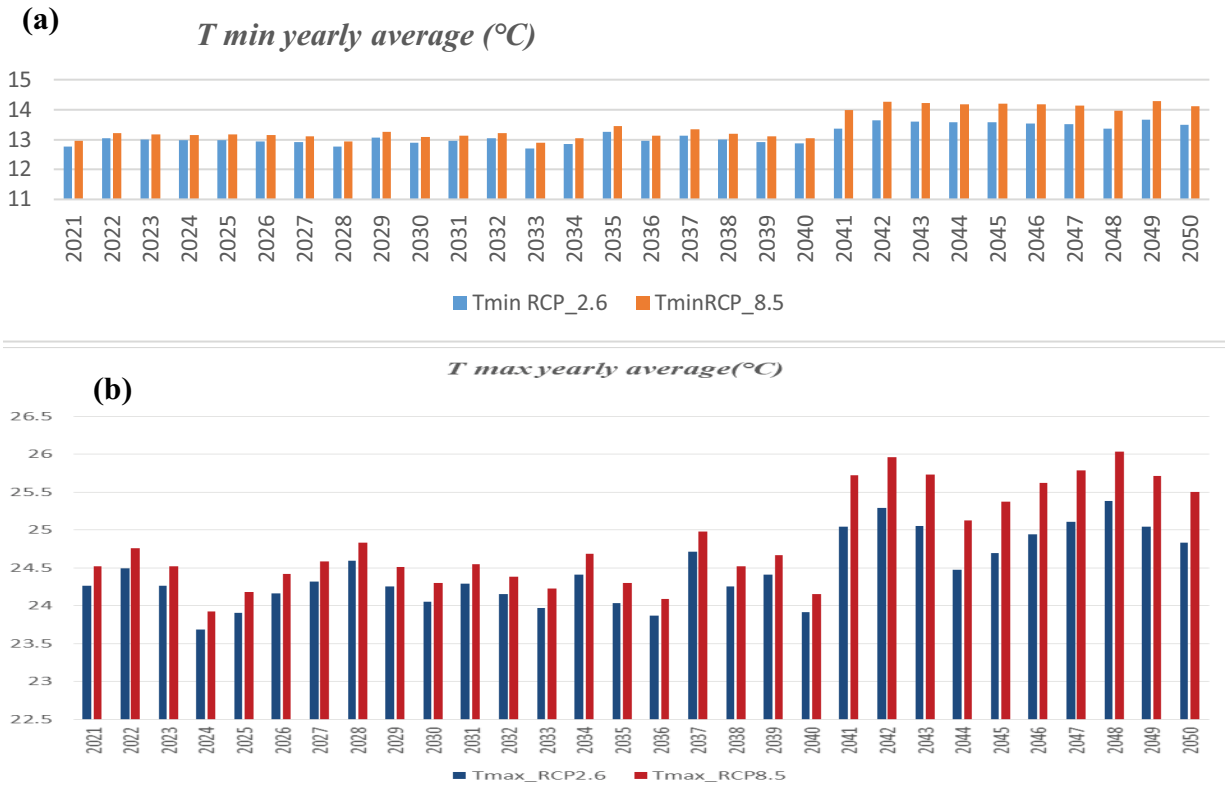

Fig. 7. Annual mean minimum (a) and maximum (b) temperature changes under RCPs scenarios.

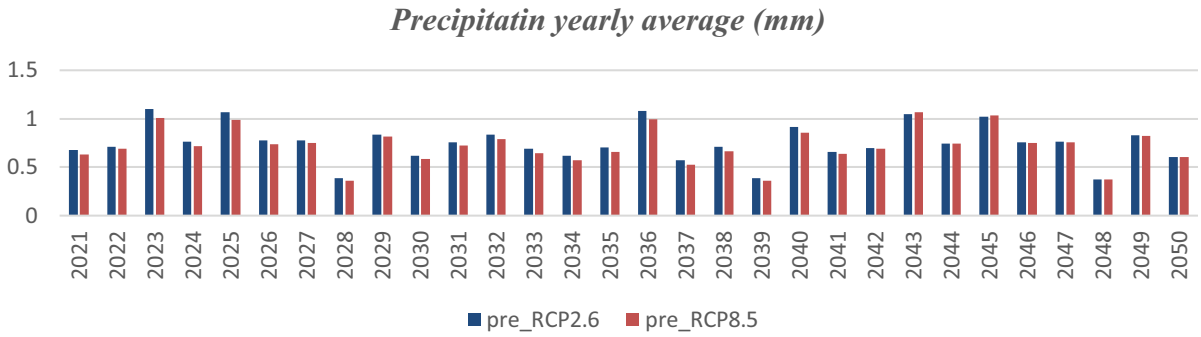

Fig. 8. Changes in the average annual precipitation under RCPs scenarios.

Fig. 13 illustrates the progression of errors during the training, validation, and testing stages. After eleven iterations using MATLAB software, the network achieved the best result with a value of 2,297.3 × 10^{-7}. At this stage, the training error was 4,341.7 × 10^{-7}, the validation error was 2,297.3 × 10^{-7}, and the test error was 6,371.2 × 10^{-6}. Additionally, Fig. 13a depicts the temporal variation of EC and the mean squared error. Another crucial aspect in assessing network accuracy is the regression between the targeted and trained outputs, which can be observed in Fig. 13b. Furthermore, Fig. 13c displays the correlation between the neural network's predicted EC outputs. The correlation coefficient for all the data points was calculated as 0.9999, indicating a strong agreement between the data predicted by the neural network and the target data.

After completing the training and testing phases and validating the accuracy of the developed neural network, data for the period from 2021 to 2050 were inputted into the neural network to predict the levels of the EC index over this 30-y timeframe. The annual and monthly averages of the EC outputs were determined and presented in Figs. 14–16, for the RCP2.6 and RCP8.5 scenarios. It was observed that the monthly mean EC concentration increases in both scenarios up until 2050 when compared to the observed data. Specifically, the highest average monthly EC concentrations were recorded as 52.06%, 81.27%, and 53.23% in March (late winter), April, and May (early spring), respectively. Conversely, the lowest average monthly EC concentrations were observed during the summer season, as shown in Fig. 14. Furthermore, in both scenarios, the average monthly

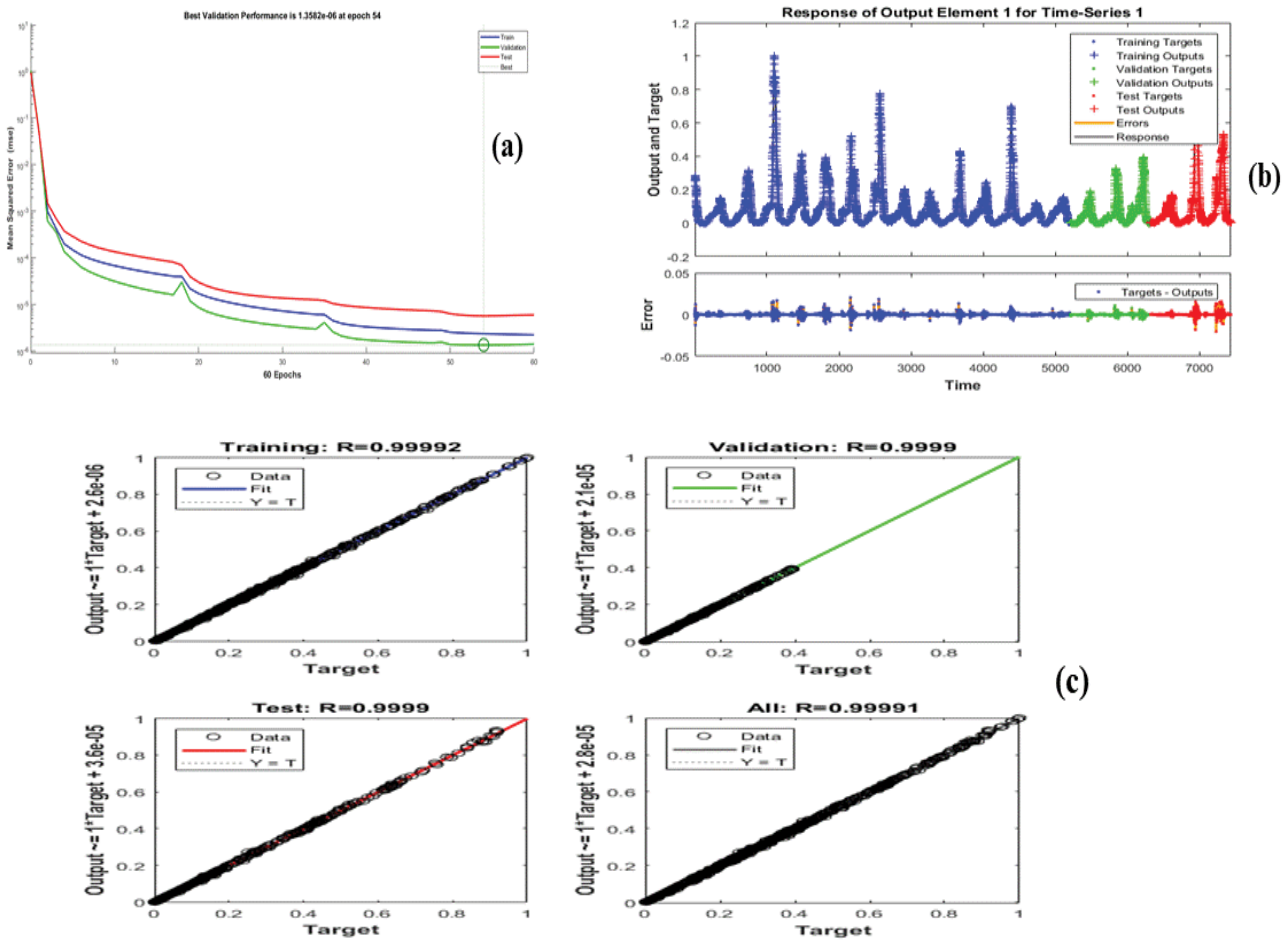

Fig. 9. (a) Mean squared error for training and test data, (b) discharge time-series and the mean squared error and (c) regression diagram between the target output and the output of the model.

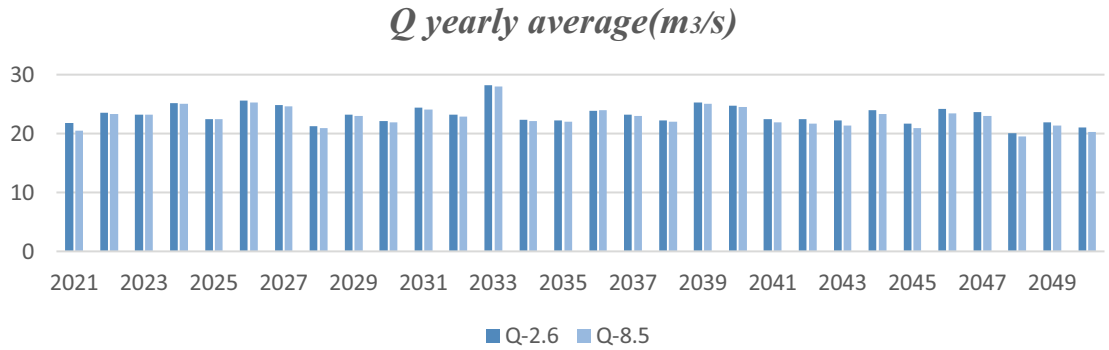

Fig. 10. Chart about the annual average of discharge (Q).

concentration of EC for all months of the year exhibits higher values when compared to the observed data (Fig. 15). The month of May stands out with the highest average monthly EC concentration, reaching 3,600 μS/cm. Moreover, the highest average annual EC concentration was projected to occur in 2048 and 2028, with concentrations of 3,628 and 3,599 μS/cm, respectively. When considering the annual mean concentrations of EC under the RCP2.6 and RCP8.5 scenarios, they increased by 24.7% and 25.1%, respectively, in comparison to the observation period (Fig. 16).

The neural network used for predicting total solid (TS) incorporates several inputs such as minimum temperature, maximum precipitation, temperature, and day of the year. The hidden layer of the neural network consists of three neurons, which were selected through a trial and error process based on minimizing the mean square error.

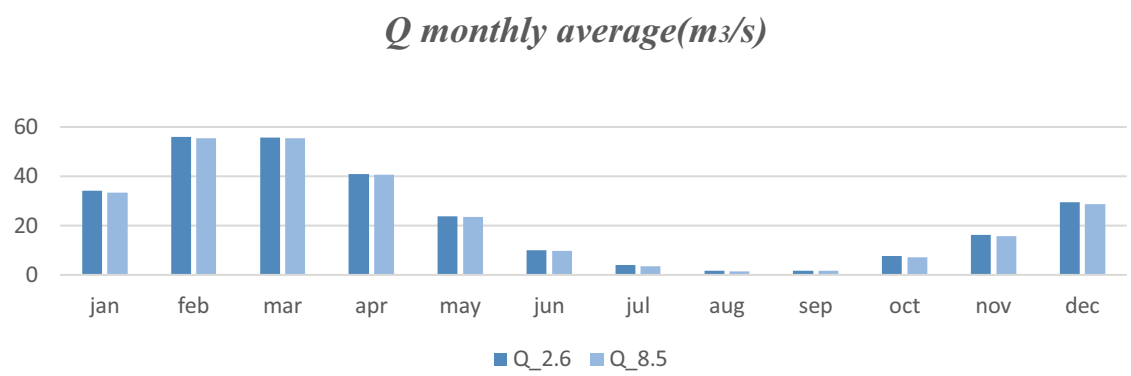

Fig. 11. Chart about the annual average of Q under RCPs scenarios.

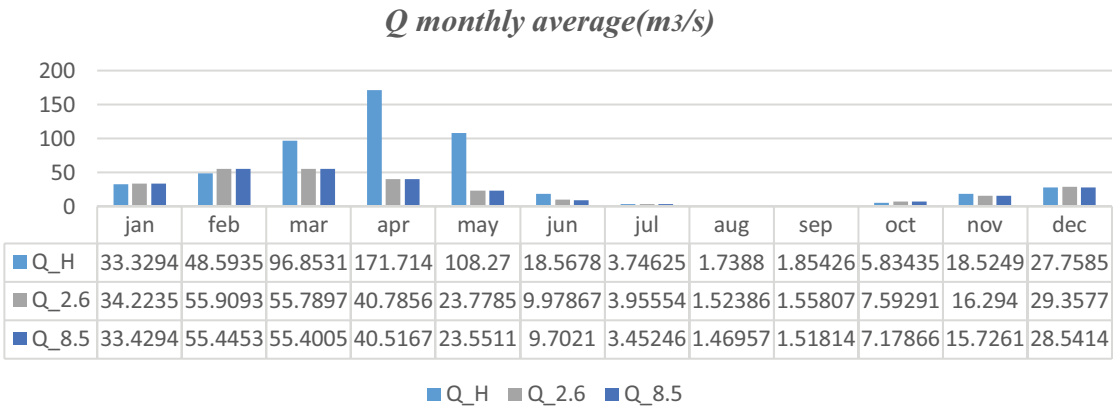

	jan	feb	mar	apr	may	jun	jul	aug	sep	oct	nov	dec
Q_H	33.3294	48.5935	96.8531	171.714	108.27	18.5678	3.74625	1.7388	1.85426	5.83435	18.5249	27.7585
Q_2.6	34.2235	55.9093	55.7897	40.7856	23.7785	9.97867	3.95554	1.52386	1.55807	7.59291	16.294	29.3577
Q_8.5	33.4294	55.4453	55.4005	40.5167	23.5511	9.7021	3.45246	1.46957	1.51814	7.17866	15.7261	28.5414

Fig. 12. Chart about monthly average Q under RCPs scenarios.

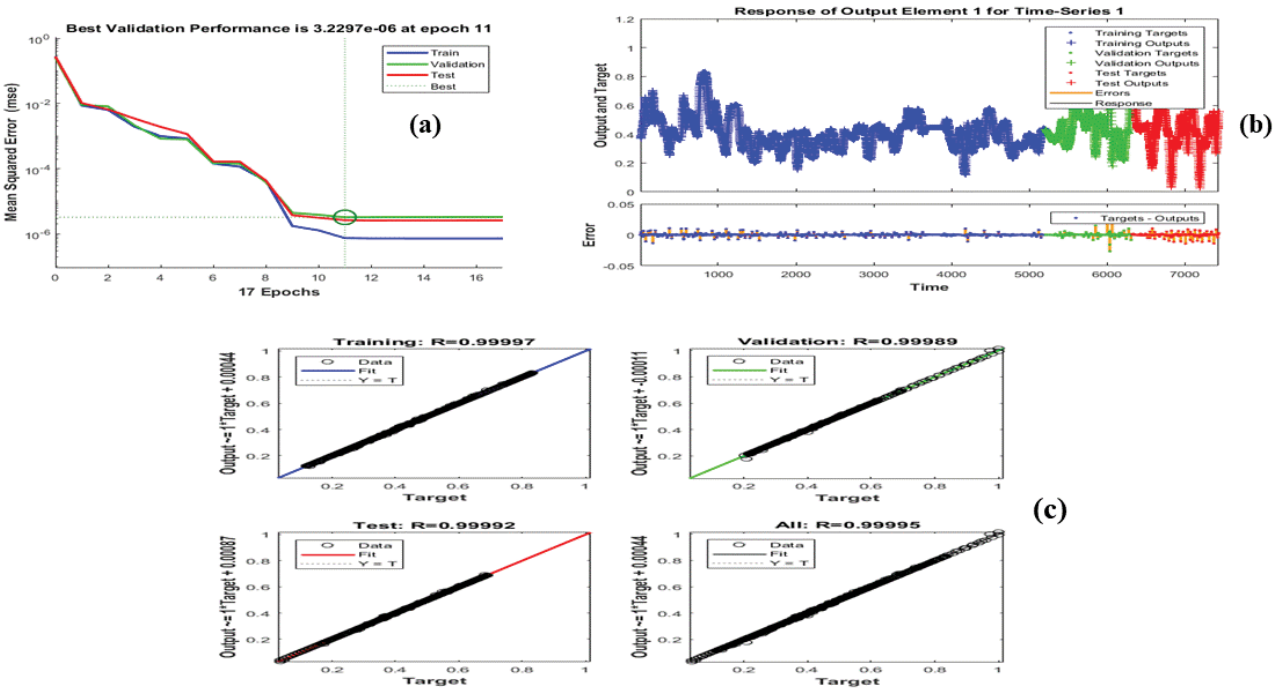

Fig. 13. (a) A network training in EC prediction, (b) time series of observed and predicted EC in the test stage and mean square error and (c) regression diagram between the target and model outputs.

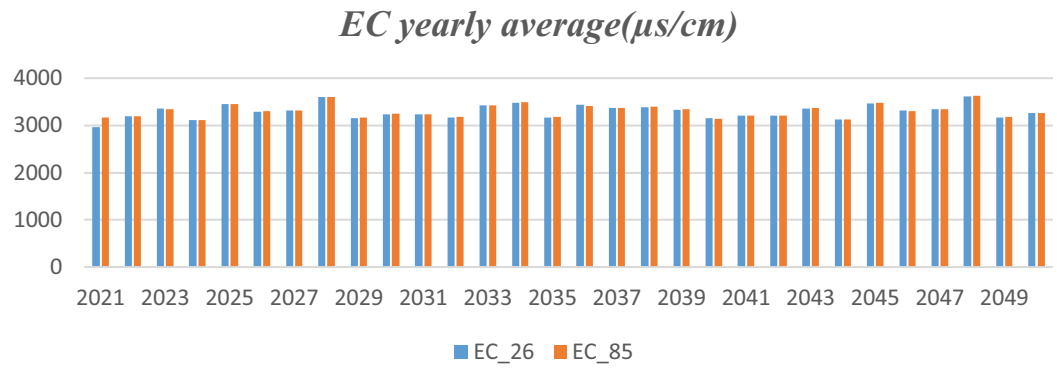

Fig. 14. Chart about the annual average of EC under RCPs scenarios.

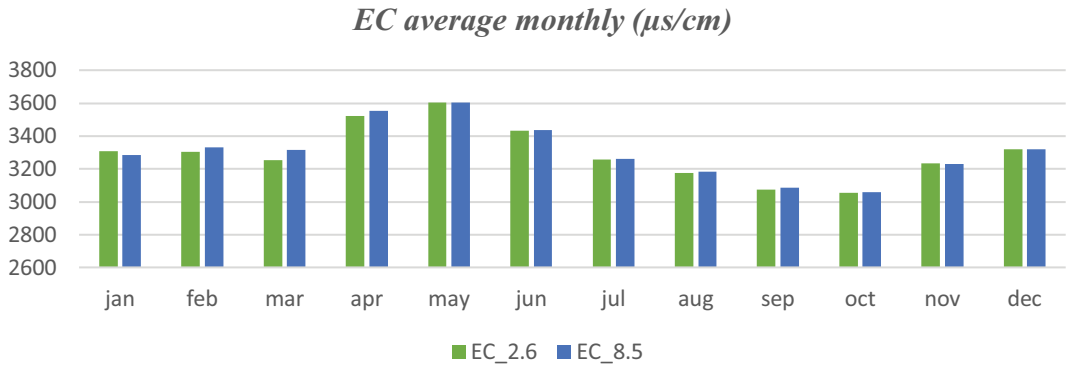

Fig. 15. Chart about the monthly average of EC under RCPs scenario.

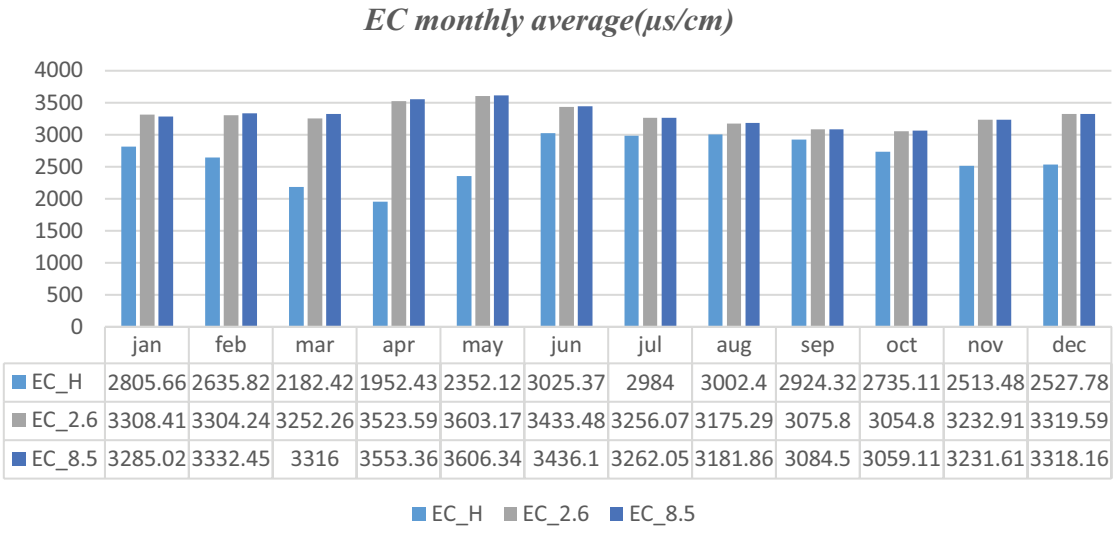

	jan	feb	mar	apr	may	jun	jul	aug	sep	oct	nov	dec
EC_H	2805.66	2635.82	2182.42	1952.43	2352.12	3025.37	2984	3002.4	2924.32	2735.11	2513.48	2527.78
EC_2.6	3308.41	3304.24	3252.26	3523.59	3603.17	3433.48	3256.07	3175.29	3075.8	3054.8	3232.91	3319.59
EC_8.5	3285.02	3332.45	3316	3553.36	3606.34	3436.1	3262.05	3181.86	3084.5	3059.11	3231.61	3318.16

Fig. 16. Monthly changes of EC for two scenarios of RCP at the beginning and end of the given period.

To account for the daily effects of past discharge on the current TS, 20 samples were chosen. Fig. 17a illustrates the decrease in errors during the training, validation, and testing stages. It is evident that the best results were achieved after 67 iterations, with a training error of 7,735.6 × 10^{-7}, a validation error of 3.0417 × 10^{-7}, and a test error of 6.9507 × 10^{-8}. Fig. 17b displays the time plot of TS and the mean squared error. Furthermore, Fig. 17c demonstrates the regression between the neural network's output and the target data. The correlation for the entire dataset was found to be 0.99994, indicating a strong agreement between the predicted data from the neural network

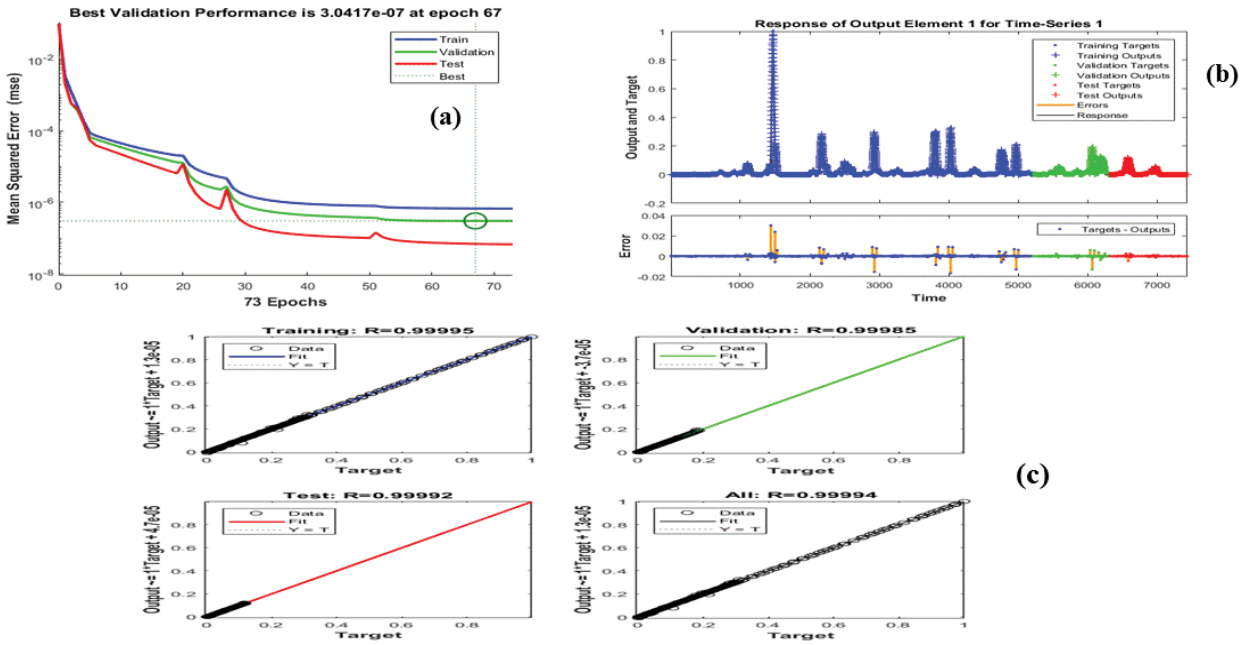

Fig. 17. (a) Mean squared error of training and test data for TS, (b) time series and mean squared error, and (c) regression plot between target and model outputs.

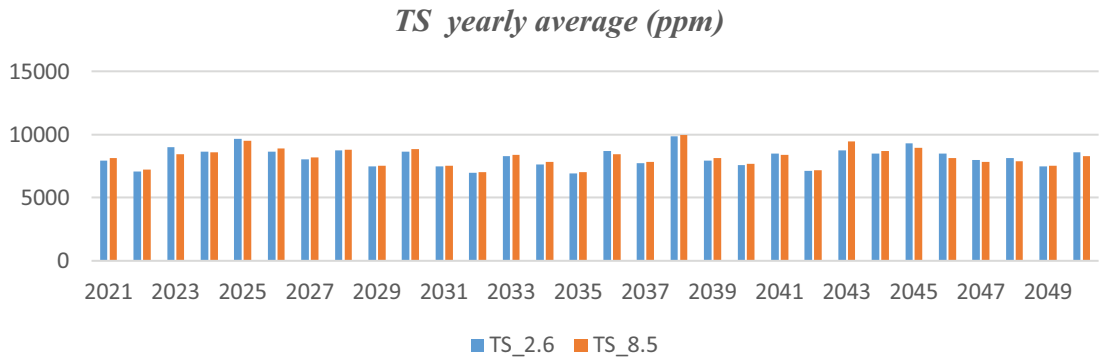

Fig. 18. Chart about the annual average of TS under RCPs scenarios.

and the observed data. The image shows a suitable linear relationship between the data points, indicating the high accuracy of the neural network in predicting TS.

According to the data collected for the studied basin, Fig. 18 displays the simulated TS amounts for the period 2021–2050 based on the RCP2.6 and RCP8.5 scenarios predicted by neural network systems. The highest annual average TS concentration was estimated to occur in 2038, reaching 10,000 ppm. On both RCP2.6 and RCP8.5 scenarios, the annual average TS concentration decreased by 45.12% and 45.04%, respectively (Fig. 19). Analyzing the data presented in Fig. 18, it is observed that the monthly average TS concentration until 2050 exhibits fluctuations in both scenarios. In comparison to the observed period, the monthly average TS concentration shows a decrease in March (late winter), April, and May (early spring). Among them, the most significant decrease occurs in April with a 90% reduction. In contrast, during January and February (early winter) and June and July (early summer), the monthly average TS concentration increases compared to the observation period (Fig. 20).

4. Discussion

In this section, we discuss the impacts of climate change on the quantity and quality of surface water, as simulated by a machine learning model. The results indicate that there will be incremental changes in seasonal and annual average temperatures under both the RCP2.6 and RCP8.5 climate emission scenarios during the future period (2021–2050). Moreover, the temperature increases projected under the RCP8.5 scenario are higher than those under the RCP2.6 scenario. According to the climate scenarios, the maximum temperature increase is expected to occur from late autumn to mid-winter, with the highest annual average temperature increase projected for 2048–2049. Reddy et al. [49] assessed

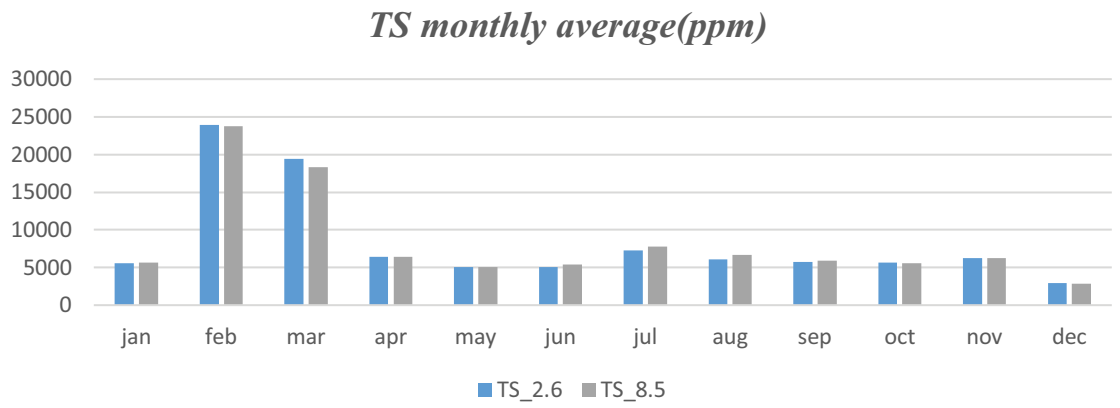

Fig. 19. Chart about the monthly average of TS under RCPs scenarios.

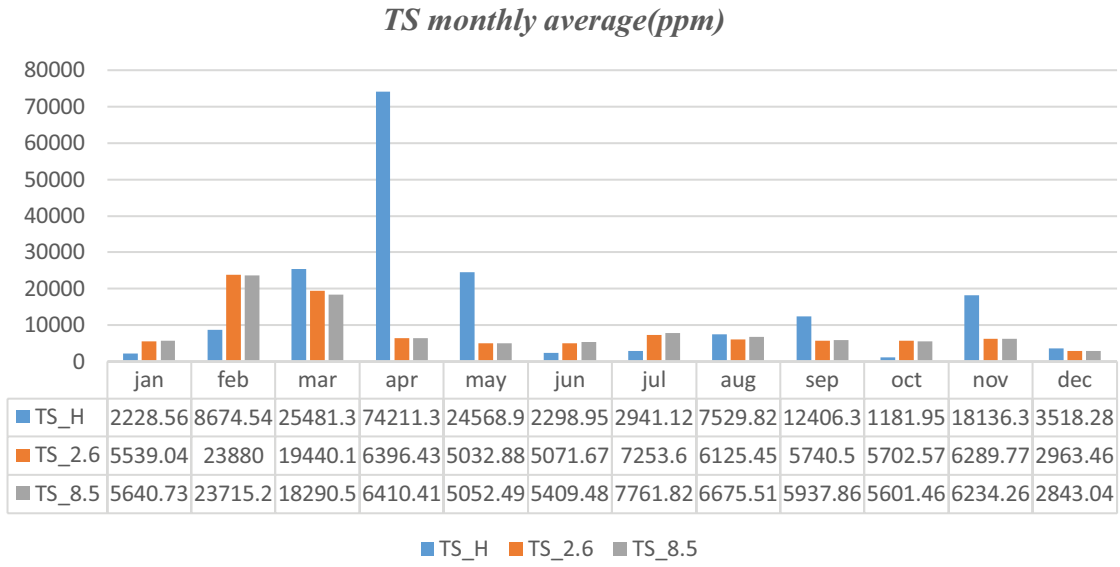

Fig. 20. Monthly changes of TS in the past and future under two scenarios of RCPs.

the potential effects of climate change using the LARS-WG model in Andhra Pradesh, a region of India. They found that the model estimated a 1%–1.53% increase in maximum temperature and a 2.5% increase in minimum temperature for the year 2030. For the year 2060, the model projected a 3.7%–10.2% increase in minimum temperature. The LARS-WG model demonstrated high efficiency and performance across all selected areas [49]. Chen et al. conducted a study to assess the effectiveness of the LARS-WG model in downscaling critical variables like daily precipitation, daily maximum temperature (T_{max}), and daily minimum temperature (T_{min}) in Sudan and South Sudan. They found that while rainfall has been decreasing in Sudan, it has been increasing in South Sudan. The model predicted an increasing trend for both minimum and maximum temperatures in the specified area [50]. In the current study, the projected levels of precipitation based on the RCP2.6 and RCP8.5 scenarios indicate that there will be increases and decreases in different seasons. Specifically, compared to the observed period, the mean monthly precipitation in February (midwinter) and April (spring) is estimated to increase by 15.38% and 18.68%, respectively, under the RCP2.6 and RCP8.5 scenarios. The highest annual average rainfall is predicted to occur in 2023, 2025, 2036, 2043, and 2045 within the next 30 y. Additionally, when comparing the flow data with the observational data, they found consistency with the changes in temperature and precipitation. Concerning seasonal changes, the amount of flow decreased significantly under both scenarios. At the end of winter, there was a decrease of 42.59%, and at the beginning of spring, there was a decrease of 77.23%. These findings align perfectly with the predicted decrease in rainfall during the same periods. The most substantial decline in the average annual flow was projected to occur in 2048. Comparing to the observed period, the RCP2.6 and RCP8.5 scenarios resulted in a decrease of 49.51% and 50.31% in the annual average flow, respectively. Our results are consistent with those reported by Reddy and Chen et al., who also employed the LARS-WG model to investigate the impact of climate change on river runoff. Furthermore, these studies estimated daily precipitation as well as daily maximum (T_{max}) and

minimum (T_{min}) temperatures [49,50]. In a study conducted by Petpongpan et al. [51], the impacts of climate change on the levels of surface and groundwater in two river basins, namely Yom and Nan, were assessed. The study's findings revealed that the average annual temperature was approximately 0.5°C–0.6°C lower than the lowest estimated temperature (under the RCP 2.6 scenario) and 0.9°C–1.0°C lower than the highest estimated temperature (under the RCP 8.5 scenario). Additionally, annual precipitation increased within the range of 20–200 mm/y under both scenarios. The total volume of water derived from surface and groundwater sources in the Yom river basin is projected to decrease under both scenarios. Specifically, there is an estimated decrease of 443.98 million·m^3/y under the RCP 2.6 scenario and a decrease of 316.77 million·m^3/y under the RCP 8.5 scenario.

Silberstein et al. [52] conducted a study investigating the relationship between climate change indicators and stream flow possibilities in southwestern Australia. According to their findings, under normal and dry weather conditions, there was a decrease in precipitation and discharge compared to the historical period, with reductions of 10% and 16%, as well as 30% and 53%, respectively. Their study also examined the simulated TS parameter for the study basin. The results indicated that the average monthly concentration of TS is increasing or decreasing in certain seasons until 2050. Specifically, during late winter and early spring, the average monthly concentration of TS decreased compared to the observed period. This reduction in the TS parameter aligns with the outcomes of their study, as it corresponds to the decrease in precipitation and discharge during those seasons. Additionally, the simulated EC parameter exhibited an increase in the monthly mean EC concentration up to 2050 in both scenarios when compared to the observed data. The greatest increase in EC concentration was associated with the RCP8.5 scenario in comparison to the observed period. In terms of seasonal changes, the highest average monthly concentration of EC is anticipated to occur with a 52.06% increase in late winter and a 27.81% increase in early spring compared to the observational data. These increases in the EC parameter are consistent with the findings of the study, considering the decrease in rainfall and discharge during late winter and early spring. Ghazi et al. [53] conducted a study using various statistical and soft-computing tools to compare predicted groundwater levels under different models, including Shared Socioeconomic Pathways (SSPs) SSP1-2.6, SSP2-4.5, and SSP5-8.5 from the Coupled Model Inter comparison Project Phase 6 (CMIP6). The study focused on Tasuj Plain in Iran, and the predictions were made for a short-term period spanning 2022–2027. The results indicated that the groundwater level in Taji Plain is projected to decrease by 3.12, 3.96, and 4.79 m based on the estimations provided by the SSP1-2.6, SSP2-4.5, and SSP5-8.5 models, respectively. Li et al. [54] conducted a study to estimate the impacts of climate change on the discharge of the Yarlung River. The findings revealed that the temperature increased by 3.8°C, while the annual average precipitation decreased by 5.8% across eight study areas. Ghazi and Jeihouni [55] investigated the variability of precipitation and temperature in the city of Tabriz, located in northwestern Iran, using data from reports by the Intergovernmental Panel on Climate Change (IPCC) spanning the period from 2015 to 2100. The results indicated that temperature is expected to rise in all months and scenarios. Average temperatures are projected to increase from 12.61°C during the base period to 13.52°C, 14.33°C, and 14.91°C under the RCP2.6, RCP4.5, and RCP8.5 scenarios, respectively. When comparing the scenarios, the predicted temperature increases were different: 15.42°C for the SSP1-2.6 scenario, 16.16°C for the SSP2-4.5 scenario, and 17.53°C for the SSP5-8.5 scenario. According to previous studies, a 11% change in rainfall primarily results in a 11%–21% change in river flows. Additionally, a temperature increases of 2°C leads to a reduction in flow ranging from 1% to 12%. Therefore, our country is not exempt from the impacts of climate change, and it is crucial to closely consider this phenomenon and its detrimental effects when planning for future adaptive measures. The results of the studies indicate that climate change will have severe and irreversible consequences, including decreased discharge, TS, and increased EC in the Qezal Ozen watershed in the upcoming periods. Consequently, all aspects of climate change impacts must be thoroughly examined to find an optimal and sustainable approach to water resource management in the basin. The present research has demonstrated that the utilization of the NARX neural network is a highly effective and reliable method for predicting surface water quality characteristics. Our findings align with those of Cai et al. [56] who also emphasized the suitability of advanced machine learning algorithms in constructing appropriate model frameworks. Furthermore, the integration of data-driven models with regional watershed properties has proven successful. Additionally, the results of Sanikhani et al. [24] indicated that the LARS-WG downscaled climatic variables effectively, and the application of machine learning models can yield reliable results when predicting water quality indices. Many studies have demonstrated that the application of machine learning models can yield reliable results when predicting water quality indices. Additionally, numerous research findings have highlighted the significant potential of machine learning algorithms in simulation and prediction [57–59].

5. Conclusion

The present study employed the NARX neural network to simulate precipitation, temperature, TS, and electrical conductivity (EC) parameters in the Ghezel Ozan River over a 30-y period (2021–2050) in Tarom City, Northwest Iran. The impact of climate change on these parameters was estimated using the HadGM2-ES models from General Circulation Models (GCM). The output models of HadGM2-ES for atmospheric variations were used to predict future climatic patterns (2050) under two scenarios: RCP2.6 and RCP8.5. Based on both scenarios, an increase in both minimum and maximum temperatures was observed until 2050, with the maximum temperature exhibiting a more significant rise under the critical RCP8.5 scenario. There were variations in rainfall changes between the RCP2.6 and RCP8.5 scenarios across different seasons. The highest decrease in precipitation was estimated to occur during mid-winter (15.38%) and early spring (18.68%) in the next period. The results obtained showed a chain of interconnected effects. As rainfall decreases, the river flow in late winter and early spring experiences significant reductions of 42.59% and 76.32%, respectively. The

relationship between precipitation, discharge, and the electrical conductivity (EC) parameter leads to an increase in the EC parameter by 52.06% and 81.27% during the late winter and early spring compared to the observed period. Overall, our findings indicate that both qualitative and quantitative water parameters are strongly influenced by climate change. Furthermore, the present study has demonstrated that the use of the NARX neural network is a highly effective and reliable method for predicting the characteristics of surface water quality.

Limitation of this study: This research did not include an extension to global climate models (GCMs), emission scenarios, or downscaling GCM output. Additionally, resampling of the data to generate sub-daily time resolution data was not conducted.

Acknowledgements

The authors acknowledge the Zanjan University of Medical Sciences, Zanjan, Iran for supporting the research.

Conflict of interest

The authors declare that they have no conflict of interest.

References

[1] A.K. Misra, Climate change and challenges of water and food security, Int. J. Sustainable Built Environ., 3 (2014) 153–165.
[2] F. Kaviari, M. Saadi Mesgari, E. Seidi, H. Motieyan, Simulation of urban growth using agent-based modeling and game theory with different temporal resolutions, Cities, 95 (2019) 102387, doi: 10.1016/j.cities.2019.06.018.
[3] S.D. Nerantzaki, D. Efstathiou, G.V. Giannakis, M. Kritsotakis, M.G. Grillakis, A.G. Koutroulis, I.K. Tsanis, N.P. Nikolaidis, Climate change impact on the hydrological budget of a large Mediterranean island, Hydrol. Sci. J., 64 (2019) 1190–1203.
[4] A. Rossati, Global warming and its health impact, Int. J. Occup. Environ. Med., 8 (2017) 7–20.
[5] Y. Tramblay, M.C. Llasat, C. Randin, E. Coppola, Climate change impacts on water resources in the Mediterranean, Reg. Environ. Change, 20 (2020 83, doi: 10.1007/s10113-020-01665-y.
[6] J. Xia, Q.-Y. Duan, Y. Luo, Z.-H. Xie, Z.-Y. Liu, X.-G. Mo, Climate change and water resources: case study of Eastern Monsoon Region of China, Adv. Clim. Change Res., 8 (2017) 63–67.
[7] Y.S. Getahun, M.-H. Li, I.-F. Pun, Trend and change-point detection analyses of rainfall and temperature over the Awash River basin of Ethiopia, Heliyon, 7 (2021) e08024, doi: 10.1016/j.heliyon.2021.e08024.
[8] R. Mahmood, S. Jia, W. Zhu, Analysis of climate variability, trends, and prediction in the most active parts of the Lake Chad basin, Africa, Sci. Rep., 9 (2019) 6317, doi: 10.1038/s41598-019-42811-9.
[9] P.-A. Versini, L. Pouget, S. McEnnis, E. Custodio, I. Escaler, Climate change impact on water resources availability: case study of the Llobregat River basin (Spain), Hydrol. Sci. J., 61 (2016) 2496–2508.
[10] S. Eslamian, F. Eslamian, Disaster Risk Reduction for Resilience: Climate Change and Disaster Risk Adaptation, Springer Nature, Cham, 2023.
[11] S. Tong, H.L. Berry, K. Ebi, H. Bambrick, W. Hu, D. Green, E. Hanna, Z. Wang, C.D. Butler, Climate change, food, water and population health in China, Bull. World Health Organ., 94 (2016) 759–765.
[12] A.J. McMichael, R.E. Woodruff, S. Hales, Climate change and human health: present and future risks, Lancet, 367 (2006) 859–869.
[13] J.M. Balbus, A.B.A. Boxall, R.A. Fenske, T.E. McKone, L. Zeise, Implications of global climate change for the assessment and management of human health risks of chemicals in the natural environment, Environ. Toxicol. Chem., 32 (2013) 62–78.
[14] X. Wang, J. Zhang, V. Babovic, Improving real-time forecasting of water quality indicators with combination of process-based models and data assimilation technique, Ecol. Indic., 66 (2016) 428–439.
[15] N. Mujere, W. Moyce, Climate Change Impacts on Surface Water Quality, in: Hydrology and Water Resource Management: Breakthroughs in Research and Practice, IGI Global, 2018, pp. 97–115.
[16] I. Delpla, A.-V. Jung, E. Baures, M. Clement, O. Thomas, Impacts of climate change on surface water quality in relation to drinking water production, Environ. Int., 35 (2009) 1225–1233.
[17] H.K. Moghaddam, A. Rajaei, Z. Rahimzadeh kivi, H.K. Moghaddam, Prediction of qualitative parameters concentration in the groundwater resources using the Bayesian approach, Groundwater Sustainable Dev., 17 (2022) 100758, doi: 10.1016/j.gsd.2022.100758.
[18] X. Wang, J. Zhang, V. Babovic, K.Y.H. Gin, A comprehensive integrated catchment-scale monitoring and modelling approach for facilitating management of water quality, Environ. Modell. Software, 120 (2019) 104489, doi: 10.1016/j.envsoft.2019.07.014.
[19] X. Li, A. Meshgi, X. Wang, J. Zhang, S.H.X. Tay, G. Pijcke, N. Manocha, M. Ong, M.T. Nguyen, V. Babovic, Three resampling approaches based on method of fragments for daily-to-subdaily precipitation disaggregation, Int. J. Climatol., 38 (2018) e1119–e1138.
[20] N. Chokkavarapu, V.R. Mandla, Comparative study of GCMs, RCMs, downscaling and hydrological models: a review toward future climate change impact estimation, SN Appl. Sci., 1 (2019) 1698, doi: 10.1007/s42452-019-1764-x.
[21] W. Fang, Q. Xue, L. Shen, V.S. Sheng, Survey on the application of deep learning in extreme weather prediction, Atmosphere, 12 (2021) 661, doi: 10.3390/atmos12060661.
[22] X. Li, V. Babovic, A new scheme for multivariate, multisite weather generator with inter-variable, inter-site dependence and inter-annual variability based on empirical copula approach, Clim. Dyn., 52 (2019) 2247–2267.
[23] N. Peleg, S. Fatichi, A. Paschalis, P. Molnar, P. Burlando, An advanced stochastic weather generator for simulating 2-D high-resolution climate variables, J. Adv. Model. Earth Syst., 9 (2017) 1595–1627.
[24] H. Sanikhani, O. Kisi, B. Amirataee, Impact of climate change on runoff in Lake Urmia basin, Iran, Theor. Appl. Climatol., 132 (2018) 491–502.
[25] P.B. Parajuli, P. Jayakody, G.F. Sassenrath, Y. Ouyang, Assessing the impacts of climate change and tillage practices on stream flow, crop and sediment yields from the Mississippi River Basin, Agric. Water Manage., 168 (2016) 112–124.
[26] Z. Hassan, S. Shamsudin, S. Harun, Application of SDSM and LARS-WG for simulating and downscaling of rainfall and temperature, Theor. Appl. Climatol., 116 (2014) 243–257.
[27] X. Li, K. Zhang, V. Babovic, Projections of future climate change in Singapore based on a multi-site multivariate downscaling approach, Water, 11 (2019) 2300, doi: 10.3390/w11112300.
[28] L. Mba, P. Meukam, A. Kemajou, Application of artificial neural network for predicting hourly indoor air temperature and relative humidity in modern building in humid region, Energy Build., 121 (2016) 32–42.
[29] A. Sharafati, S.B. Haji Seyed Asadollah, D. Motta, Z.M. Yaseen, Application of newly developed ensemble machine learning models for daily suspended sediment load prediction and related uncertainty analysis, Hydrol. Sci. J., 65 (2020) 2022–2042.
[30] S. Marabi, M. Hafezparast, Quantitative qualitative prediction of Khorramrud River discharge due to climate change with Neurosolution model and support vector regression, Irrig. Water Eng., 12 (2021) 291–313.
[31] N.A. Mohammed, A. Al-Bazi, An adaptive backpropagation algorithm for long-term electricity load forecasting, Neural Comput. Appl., 34 (2022) 477–491.

[32] D. Niu, F. Wu, S. Dai, S. He, B. Wu, Detection of long-term effect in forecasting municipal solid waste using a long short-term memory neural network, J. Cleaner Prod., 290 (2021) 125187, doi: 10.1016/j.jclepro.2020.125187.
[33] S. Emamgholizadeh, H. Kashi, I. Marofpoor, E. Zalaghi, Prediction of water quality parameters of Karoon River (Iran) by artificial intelligence-based models, Int. J. Environ. Sci. Technol., 11 (2014) 645–656.
[34] N.M. Gazzaz, M.K. Yusoff, A.Z. Aris, H. Juahir, M.F. Ramli, Artificial neural network modeling of the water quality index for Kinta River (Malaysia) using water quality variables as predictors, Mar. Pollut. Bull., 64 (2012) 2409–2420.
[35] N.M. Gazzaz, M.K. Yusoff, M.F. Ramli, H. Juahir, A.Z. Aris, Artificial neural network modeling of the water quality index using land use areas as predictors, Water Environ. Res., 87 (2015) 99–112.
[36] K. Sulaiman, L.H. Ismail, M.A.M. Razi, M.S. Adnan, R. Ghazali, Water quality classification using an artificial neural network (ANN), IOP Conf. Ser.: Mater. Sci. Eng., 601 (2019) 012005, doi: 10.1088/1757-899X/601/1/012005.
[37] M. Al-Mukhtar, F. Al-Yaseen, Modeling water quality parameters using data-driven models, a case study Abu-Ziriq marsh in south of Iraq, J. Hydrol., 6 (2019) 24, doi: 10.3390/hydrology6010024.
[38] A.K. Kadam, V.M. Wagh, A.A. Muley, B.N. Umrikar, R.N. Sankhua, Prediction of water quality index using artificial neural network and multiple linear regression modelling approach in Shivganga River basin, India, Model. Earth Syst. Environ., 5 (2019) 951–962.
[39] N. Jafarzadeh, S. Ahmad Mirbagheri, T. Rajaee, A. Danehkar, M. Robati, Using artificial intelligent to model predict the biological resilience with an emphasis on population of cyanobacteria in Jajrood River in The Eastern Tehran, Iran, J. Environ. Health Sci. Eng., 20 (2022) 123–138.
[40] J. Aazami, N. KianiMehr, A. Zamani, Ecological water health assessment using benthic macroinvertebrate communities (case study: the Ghezel Ozan River in Zanjan Province, Iran), Environ. Monit. Assess., 191 (2019) 689, doi: 10.1007/s10661-019-7894-1.
[41] S. Fatichi, V.Y. Ivanov, E. Caporali, Simulation of future climate scenarios with a weather generator, Adv. Water Resour., 34 (2011) 448–467.
[42] C. Miao, Q. Duan, Q. Sun, J. Li, Evaluation and application of Bayesian multi-model estimation in temperature simulations, Prog. Phys. Geogr., 37 (2013) 727–744.
[43] C.W. Richardson, Stochastic simulation of daily precipitation, temperature, and solar radiation, Water Resour. Res., 17 (1981) 182–190.
[44] K. Duan, Y. Mei, A comparison study of three statistical downscaling methods and their model-averaging ensemble for precipitation downscaling in China, Theor. Appl. Climatol., 116 (2014) 707–719.
[45] S. Moghanlo, M. Alavinejad, V. Oskoei, H.N. Saleh, A.A. Mohammadi, H. Mohammadi, Z. DerakhshanNejad, Using artificial neural networks to model the impacts of climate change on dust phenomenon in the Zanjan region, north-west Iran, Urban Clim., 35 (2021) 100750, doi: 10.1016/j.uclim.2020.100750.
[46] J.M. Melillo, T. Richmond, G. Yohe, Climate Change Impacts in the United States, Third National Climate Assessment, 2014.
[47] E. Pisoni, M. Farina, C. Carnevale, L. Piroddi, Forecasting peak air pollution levels using NARX models, Eng. Appl. Artif. Intell., 22 (2009) 593–602.
[48] Y. Chen, L. Song, Y. Liu, L. Yang, D. Li, A review of the artificial neural network models for water quality prediction, Appl. Sci., 10 (2020) 5776, doi: 10.3390/app10175776.
[49] K.S. Reddy, M. Kumar, V. Maruthi, B. Umesha, Vijayalaxmi, C.V.K. Nageswar Rao, Climate change analysis in southern Telangana region, Andhra Pradesh using LARS-WG model, Curr. Sci., 107 (2014) 54–62.
[50] H. Chen, J. Guo, Z. Zhang, C.-Y. Xu, Prediction of temperature and precipitation in Sudan and South Sudan by using LARS-WG in future, Theor. Appl. Climatol., 113 (2013) 363–375.
[51] C. Petpongpan, C. Ekkawatpanit, D. Kositgittiwong, Climate change impact on surface water and groundwater recharge in Northern Thailand, Water, 12 (2020) 1029, doi: 10.3390/w12041029.
[52] R.P. Silberstein, S.K. Aryal, J. Durrant, M. Pearcey, M. Braccia, S.P. Charles, L. Boniecka, G.A. Hodgson, M.A. Bari, N.R. Viney, D.J. McFarlane, Climate change and runoff in south-western Australia, J. Hydrol., 475 (2012) 441–455.
[53] B. Ghazi, E. Jeihouni, O. Kisi, Q.B. Pham, B. Đurin, Estimation of Tasuj aquifer response to main meteorological parameter variations under shared socioeconomic pathways scenarios, Theor. Appl. Climatol., 149 (2022) 25–37.
[54] F. Li, Z. Xu, W. Liu, Y. Zhang, The impact of climate change on runoff in the Yarlung Tsangpo River basin in the Tibetan Plateau, Stochastic Environ. Res. Risk Assess., 28 (2014) 517–526.
[55] B. Ghazi, E. Jeihouni, Projection of temperature and precipitation under climate change in Tabriz, Iran, Arabian J. Geosci., 15 (2022) 621, doi: 10.1007/s12517-022-09848-z.
[56] H. Cai, H. Shi, S. Liu, V. Babovic, Impacts of regional characteristics on improving the accuracy of groundwater level prediction using machine learning: the case of central eastern continental United States, J. Hydrol.: Reg. Stud., 37 (2021) 100930, doi: 10.1016/j.ejrh.2021.100930.
[57] S. Jiang, Y. Zheng, C. Wang, V. Babovic, Uncovering flooding mechanisms across the contiguous United States through interpretive deep learning on representative catchments, Water Resour. Res., 58 (2022) e2021WR030185, doi: 10.1029/2021WR030185.
[58] H.M.V.V. Herath, J. Chadalawada, V. Babovic, Hydrologically informed machine learning for rainfall–runoff modelling: towards distributed modelling, Hydrol. Earth Syst. Sci., 25 (2021) 4373–4401.
[59] J. Chadalawada, H.M.V.V. Herath, V. Babovic, Hydrologically informed machine learning for rainfall-runoff modeling: a genetic programming-based toolkit for automatic model induction, Water Resour. Res., 87 (2015) 99–112.